specifications. The proposed dual-broadband semicircle slot antenna also provides the frequency ratio of two operating modes tuned in the range of 2.2–3.1. The measured peak antenna gains for the operating frequencies across dual WLAN bands are measured to be, respectively, 4.7 and 4.9 dBi with the gain variations within 0.5 dBi.

ACKNOWLEDGMENT

This article was supported by the National Science Council (NSC), Taiwan, Republic of China, under Grant NSC91–2622-E-022–002-CC3.

REFERENCES

1. H.G. Akhavan and D.M. Syahkal, Study of coupled slot antennas fed by microstrip lines, In 10th International Conference on Antennas and Propagation, Edinburgh, UK, April 14–17, 1997, pp. 1290–1292.
2. S.Y. Lin and K.L. Wong, A dual-frequency microstrip-line-fed printed slot antenna, Microwave Opt Technol Lett 28 (2001), 373–375.
3. T. Morioka, S. Araki, and K. Hirasawa, Slot antenna with parasitic element for dual band operation, Electron Lett 33 (1997), 2093–2094.
4. C.J. Wang and W.T. Tsai, A stair-shaped slot antenna for the triple-band WLAN applications, Microwave Opt Technol Lett 39 (2003), 370–372.
5. J.W. Wu, H.M. Hsiao, J.H. Lu, and S.H. Chang, Dual-broadband design of rectangular slot antenna for 2.4/5 GHz wireless communication, Electron Lett 40 (2004), 1461–1463.
6. H.M. Hsiao, J.W. Wu, Y.D. Wang, J.H. Lu, and S.H. Chang, Novel dual-broadband rectangular slot antenna for 2.4/5 GHz wireless communication, Microwave Opt Technol Lett 46 (2005), 197–201.
7. Ansoft Corporation. HFSS version 10.0, Ansoft Software Inc., 2006.

EFFECT OF Li/Nb RATIO ON HOLOGRAPHIC STORAGE PROPERTIES OF In:$LiNbO_3$ CRYSTALS

Yiran Nie,[1] Rui Wang,[2] and Biao Wang[1,3]

[1] Department of Aerospace Engineering and Mechanics, Electro-Optics Technology Center, Harbin Institute of Technology, Harbin 150001, People's Republic of China

[2] Department of Applied Chemistry, Electro-Optics Technology Center, Harbin Institute of Technology, Harbin 150001, People's Republic of China

[3] State Key Laboratory of Optoelectronic Materials and Technologies, School of Physics and Engineering, Sun Yat-Sen University, Guangzhou 510275, People's Republic of China

Received 11 February 2007

ABSTRACT: *In:$LiNbO_3$ crystals with different Li/Nb ratios in the melts (Li/Nb = 0.94, 1.0, 1.1, 1.2) have been grown. The changes of the crystal structure on the Li/Nb were analyzed by the ultraviolet–visible absorption spectra. The holographic storage properties of In:$LiNbO_3$ crystals were investigated by two-wave coupling technique. The diffraction efficiency, response time, and photoconductivity of the crystals were measured. With increase in the ratio of Li/Nb, the diffraction efficiency decreases, the response time shortens, and the photoconductivity increases.* © 2007 Wiley Periodicals, Inc. Microwave Opt Technol Lett 49: 2169–2171, 2007; Published online in Wiley InterScience (www.interscience.wiley.com). DOI 10.1002/mop.22669

Key words: *In:$LiNbO_3$; Li/Nb ratio; crystal growth; absorption spectra; holographic storage*

1. INTRODUCTION

$LiNbO_3$ crystal possesses excellent electro-optic, acousto-optic, and nonlinear optical properties [1]. It is a promising material used in holographic storage for its excellent photorefractive properties [2, 3]. However, $LiNbO_3$ crystal has two shortcomings, the long response time and weak photodamage resistant ability, which restrict its applications. The photodamage resistant ability of the $LiNbO_3$ crystal can be greatly improved by doping with MgO [4], ZnO [5], or In_2O_3 [6], Sc_2O_3 [7]. On the other hand, the intrinsic defects existing in $LiNbO_3$ crystal will reduce with increase in the Li content, and many optical properties will be changed accordingly [8].

In this article, we propose to grow In:$LiNbO_3$ crystals with various ratios of Li/Nb. In^{3+} ions doping and Li content increasing are applied to improve the photodamage resistant ability and to shorten the response time. The influences of Li/Nb ratios on the ultraviolet–visible absorption spectra and the holographic storage properties (diffraction efficiency, response time, and photoconductivity) are investigated.

2. EXPERIMENTAL

2.1. Samples Preparation

A series of In:$LiNbO_3$ crystals were grown from the melt with various ratio of Li/Nb from 0.94 to 1.2 by the Czochralski method with the intermediate frequency furnace as the heater. A pure congruent $LiNbO_3$ crystal was also grown for comparison. The composition and the growth conditions were shown in Table 1. The starting materials were Li_2CO_3, Nb_2O_5, and In_2O_3 with a purity of 99.99%. To prepare polycrystalline materials, the raw materials were mixed thoroughly. Then, the raw materials were filled in a platinum crucible, calcined at 850°C for 4 h, and sintered at 1150°C for 4 h. All the crystals were grown along the *c*-axis. The as-grown crystals were poled in another furnace where the temperature was at about 1200°C for 4 h with a direct current of 5 mA/cm^2. Then, the crystals were cut into wafers and all the samples were polished to optical grade.

TABLE 1 Composition and Growth Condition of In:$LiNbO_3$ With Different Li/Nb Ratios

	Sample no.				
	1	2	3	4	5
Li/Nb (mol ratio)	0.94	0.94	1.0	1.1	1.2
In (mol %)	0	1	1	1	+1
Pulling rate (mm/h)	1.5	1.5	1.0	0.5	0.3
Rotation rate (rpm)	25	25	20	15	12
Temperature gradient (°C)	40	40	35	30	20
Crystal size (mm^3)	Φ30 × 40	Φ30 × 35	Φ30 × 35	Φ20 × 30	Φ20 × 20
Wafer size (mm^3)	10 × 2 × 10	10 × 2 × 10	10 × 2 × 10	10 × 2 × 10	10 × 2 × 10

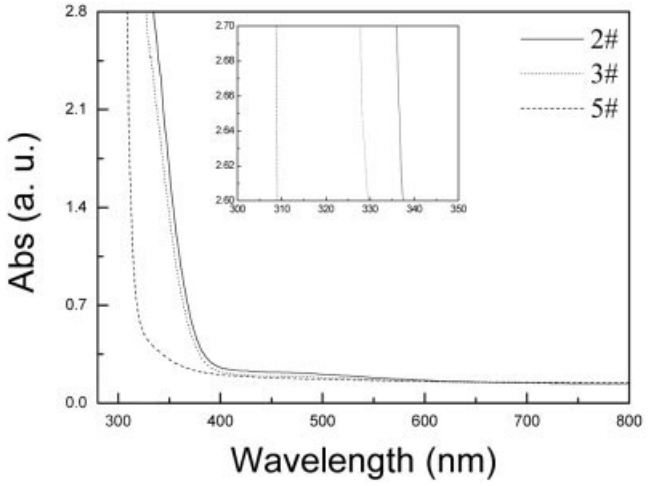

Figure 1 Ultraviolet–visible absorption spectra of samples

2.2. Measurements of the Absorption Spectra

The ultraviolet–visible spectrophotometer of CARY mode was used to measure the absorption spectra of the samples. The wavelength range was from 300 to 1000 nm. The result was shown in Figure 1.

2.3. Measurements of Holographic Storage Properties

The diffraction efficiency and the response time of the In:$LiNbO_3$ crystals were measured by the two-wave coupling experiments. The optical path was shown in Figure 2. The He–Ne laser (λ = 632.8 nm) was used as the light source in the experiment. The polarization of the output beam was in the incident plane. The beam was separated into two by the beam splitter. One is signal light I_s and the other is reference light I_r. The intensity of $I_r = I_s$ = 150 mW/cm^2 and their crossing angle is 10–20°.

3. RESULTS AND DISCUSSIONS

Figure 1 shows the ultraviolet–visible absorption spectra of the In:$LiNbO_3$ crystals with different Li/Nb ratios. It can be seen that the absorption edges of the In:$LiNbO_3$ crystal shift to violet with increasing the ratio of Li/Nb.

The principal structure of $LiNbO_3$ crystal is formed by oxygen octahedron. The optical absorption edge is decided by the valence-electron energy from the 2p-orbits of O^{2-} to the 4d-orbits of Nb^{5+}. So the valence-electronic state of O^{2-} directly affects the site of the absorption edge. If the O^{2-} polarization ability increases, the energy for the electron transition decreases and the absorption edge shifts to infrared. On the contrary, the absorption

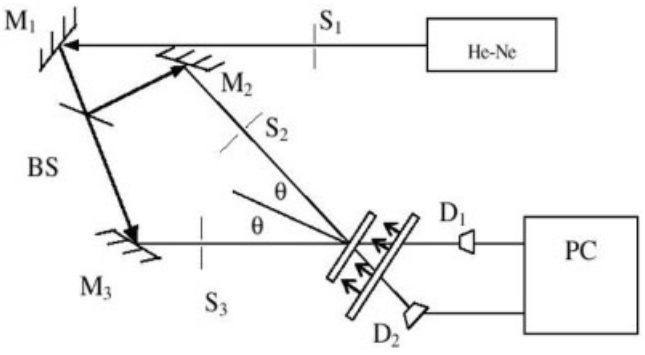

Figure 2 Sketch of two-wave coupling optical path

TABLE 2 Holographic Properties of the Samples

Sample no.	η_{max} (%)	τ (s)	σ_{ph} ($\times 10^{-15}$ Ω^{-1} cm^{-1})
1	32.4	568	2.8
2	22.6	294	3.4
3	19.7	128	3.8
4	9.7	86	4.3
5	6.4	27	6.7

edge shifts to violet. From the viewpoint of Li-vacancy model, there are Li^+ vacancies in congruent pure $LiNbO_3$ crystal and the Li^+ vacancies are filled by Nb^{5+} to form antisite defects $(Nb_{Li})^{4+}$ [9, 10]. In the case of In:$LiNbO_3$ crystals, the In^{3+} concentration is invariable and the $(Nb_{Li})^{4+}$ concentration reduces with increasing the ratio of Li/Nb. The decrease in $(Nb_{Li})^{4+}$ leads to the polarization ability of O^{2-} decreasing and the electron transition energy increasing. So the absorption edges of In:$LiNbO_3$ crystals are shifted to violet with increase in the ratio of Li/Nb.

The diffraction efficiency is one important parameters for crystal used in holographic storage. The diffraction efficiency η is defined as the ratio of the diffracted light intensity I_{sd} to the transmitted light intensity I_{st} for the signal light, i.e.,

$$\eta = \left(\frac{I_{sd}}{I_{st}}\right) \times 100\% \tag{1}$$

The response time τ is defined as the time from the light begins radiating to the time that the diffraction efficiency η is up to $(1 - e^{-1})$ of its maximum (η_{max}).

By the logarithmic transformation of the diffraction efficiency to the diffusion field, the later equation can be gotten [11],

$$\ln(\eta/\eta_{max}) = \frac{2\sigma_{ph}}{\varepsilon} t + \text{constant} \tag{2}$$

where η_{max} is the maximum of the diffraction efficiency, σ_{ph} is the photoconductivity, and ε is the dielectric constant of the material. It can be seen from Eq. (2) that σ_{ph} is the slope rate of the line $\ln(\eta/\eta_{max}) \sim 2t/\varepsilon$. The results of the holographic storage properties of In:$LiNbO_3$ are shown in Table 2.

As can be seen from the results, with increase in the ratios of Li/Nb, the photoconductivity increases, response time is shortened, and the diffraction efficiency decreases. In the In:$LiNbO_3$ crystals, the photoconductivity is related to the electron traps $(Nb_{Li})^{4+}$. The decrease in $(Nb_{Li})^{4+}$ with increase in the Li/Nb ratio leads to the increasing of the photoconductivity σ_{ph}.

The relationship of diffraction efficiency η_{max}, response time τ, and conductivity σ_{ph} can be described as follows

$$\tau = \frac{\varepsilon\varepsilon_0}{4\pi\sigma} \tag{3}$$

where $\varepsilon\varepsilon_0$ is the dielectric constant and σ is the conductivity [12].

$$\eta_{max} = \sin^2\left(\frac{\pi dB\kappa\alpha I}{\sigma\lambda\cos\theta}\right) \tag{4}$$

where d is the thickness, B is the generalized electro-optical coefficient, κ is the glass constant, α is the optical absorption, I is the intensity of the light, λ is the wavelength, θ is the incident angle, and σ is the conductivity ($\sigma = \sigma_d + \sigma_{ph}$; σ_d is the dark

conductivity and σ_{ph} is the photoconductivity, $\sigma_d \ll \sigma_{ph}$, so $\sigma \approx \sigma_{ph}$) [13, 14].

From the formulas (3) and (4), we can see that the diffraction efficiency and the response time are inversely proportional to the conductivity σ. So the photoconductivity σ_{ph} increases with the increase in Li/Nb ratio. The diffraction efficiency decreases and response time shortens simultaneously.

4. CONCLUSIONS

In:$LiNbO_3$ crystals have been grown from the melt with various ratios of Li/Nb. With increase in the ratios of Li/Nb, the absorption edge shifts to violet, the photoconductivity increases, response time shortens, and the diffraction efficiency decreases a little. All these are induced by the intrinsic defects decreasing in In:$LiNbO_3$ crystals. In:$LiNbO_3$ crystals grown from high Li/Nb melt with good quality are more promising materials used in the holographic storage than congruent In:$LiNbO_3$ crystals.

ACKNOWLEDGMENT

This article was supported by the National Natural Science Foundation of China (50232030, 10572155, 10172030) and the Science Foundation of Guangzhou Province (2005A10602002).

REFERENCES

1. P. Guner and J.P. Huignard, Photorefractive materials and their application, Vol. 62: Topics of applied physics, , Springer, Berlin, 1998.
2. L. Hesselink, S.S. Orlov, A. Liu, A. Akella, D. Lande, and R.R. Neurggaonkar, Photorefractive materials for nonvolatile volume holographic storage, Science 282 (1998), 1089–1094.
3. D.V. Linde, A.M. Glass, and K.F. Rodgers, Optical storage using refractive index changes induced by two-step excitation, J Appl Phys 47 (1976), 217–220.
4. D.A. Bryan, R. Gerson, and H.E. Tomaschke, Increased optical damage resistance in lithium niobate, Appl Phys Lett 44 (1984), 847–849.
5. T.R. Volk, V.I. Pryalkin, and N.M. Rubinina, Optical-damage-resistant $LiNbO_3$:Zn crystal, Opt Lett 15 (1990), 996–998.
6. Y. Kong, J. Wen, and H. Wang, New doped lithium niobate crystal with high resistance to photorefraction-$LiNbO_3$:In, Appl Phys Lett 66 (1995), 280–281.
7. J.K. Yamamoto, K. Kitamura, N. Lyi, S. Kimura, Y. Furukawa, and M. Sato, Increased optical damage resistance in Sc_2O_3-doped $LiNbO_3$, Appl Phys Lett 61 (1992), 2156–2158.
8. Y. Furukawa, M. Sato, K. Kitamura, Y. Yajima, and M. Minakara, Optical damage resistance and crystal quality of $LiNbO_3$ single crystals with various [Li]/[Nb] ratios, J Appl Phys 72 (1992), 3250–3254.
9. N. Iyi, K. Kitamura, F. Izumi, J.K. Yamamoto, T. Hayashi, H. Asano, and S. Kimura, Comparative study of defect structures in lithium niobate with different compositions, J Solid State Chem 101 (1992), 340–352.
10. A. Yatsenko, H. Maksimova, and N. Sergeev, NMR study of intrinsic defects in congruent lithium niobate, Cryst Res Technol 34 (1999), 709–713.
11. M.P. Bienvenu, D. Woodbury, and T.A. Rabson, Hologram decay in $LiNbO_3$:Fe with a time varying conductivity, J Appl Phys 51 (1980), 4245–4247.
12. G.C. Valley and M.B. Klein, Optical properties of photorefractive materials for optical data processing, Opt Eng 22 (1983), 704–711.
13. N.V. Kukhtarev, V.B. Markov, and S.G. Odulov. Holographic storage in electrooptic crystals. I. Steady state, Ferroelectrics 24 (1979), 949–960.
14. T. Volk, N. Rubinina, and M. Wöhlecke, Optical-damage-resistant impurities in lithium niobate, J Opt Soc Am B 11 (1994), 1681–1687.

A HALF-MOON ANTENNA WITH TILT ANGLES FOR WIDEBAND APPLICATIONS

Chang Won Jung and Yongjin Kim
Embedded Systems Solution Laboratory, Samsung Advanced Institute of Technology, Mt. 14–1, Nongseo-Dong, Giheung-Gu, Yongin-Si, Gyeonggi-Do, Korea 446–712

Received 19 February 2007

ABSTRACT: *A half-moon antenna is presented for wideband communication system. The proposed antenna radiates linear polarized wave omnidirectionally in wide frequency band from 1.5 GHz to more than 5 GHz (>~110%). The frequency bands of the proposed antenna are investigated from the variable current path lengths by tilting angles. The overall radiation gain of the proposed antenna is 2–3 dBi.* © 2007 Wiley Periodicals, Inc. Microwave Opt Technol Lett 49: 2171–2174, 2007; Published online in Wiley InterScience (www.interscience.wiley.com). DOI 10.1002/mop.22656

Key words: *half-moon antenna; tilt angle; wideband antenna; omnidirectional radiation*

1. INTRODUCTION

Patch antennas are broadly used in wireless communications because of the following characteristics: low profile, low cost, and ease of fabrication [1–3]. However, it is well known that the bandwidth of patch antennas is narrow [1–3]. As an example, for triple-band option, more than 30% of the operating bandwidth is required [4]. Bandwidth in excess of 70% can be achieved with aperture-coupled stacked patches [4]. However, such configurations occupy considerable space and are not always acceptable for integration with other circuitry. Thus, many attempts have been made to widen the bandwidth of printed antennas within specified dimensions [4–6]. There are several types of antennas that exhibit large bandwidths such as bowtie, spiral, planar-monopole antenna. These can be easily constructed using inexpensive printed circuit board (PCB) technology. Also, a half-moon antenna as a planar-monopole antenna is introduced recently for the wideband antenna applications in high frequency band (11–14 GHz) [7].

In this letter, we use a semicircular antenna. It is one of the promising candidates for wideband applications by variable current path lengths of the semicircle. The semicircle is tilted starting from the center feed to lower the frequency band operation. The proposed antenna satisfies the omnidirectional radiation and linear polarization requirements for the commercial wireless communication systems.

2. DESIGN OF THE HALF-MOON ANTENNA

2.1 Operation Frequency Band

The proposed half-moon antenna printed on Roger's TMM3 (ε_r = 3.27, tan δ = 0.002) PCB is shown in Figure 1. The thickness of PCB is 3.175 mm (h). The semicircle is printed and is fed by coplanar waveguide (CPW), which has a width (W) of 4.95 and 0.225 mm of gap between the signal line and ground plane. Length (l_c) of CPW is 30 mm. The diameter (D) of semicircle is 50 mm. Therefore, radius (r) is 25 mm. The antenna has tilt angles ($\alpha°$) to investigate the variation of the operation frequency bands by tilt angles.

The vectors of surface current on the half-moon are simulated using HFSS (FEM), and the surface current paths are also shown in Figure 2. The shortest current path from the center feed-point